Food & Function

ROYAL SOCIETY OF CHEMISTRY

PAPER

View Article Online
View Journal

Check for updates

Cite this: DOI: 10.1039/d6fo00279j

Oleic and omega-3 fatty acids buffer neuroinflammation in a scopolamine model with Alzheimer's-like features *via* target-level interactions

Marlua Albertuni,[a] Maria Torrecillas-Lopez,[a,b] Teresa Gonzalez-de la Rosa,[a,b] Luna Barrera-Chamorro,[a,b] Elvira Marquez-Paradas,[a,b] Jose L. del Rio-Vazquez,[a] Maria D. Navarro-Hortal,[a] Carmen M. Claro-Cala *[b,c] and Sergio Montserrat-de la Paz [a,b]

Diet quality, beyond total fat, may shape the immune tone of the brain in Alzheimer's-relevant contexts. We examined whether the fatty acid profile and food matrix of high-fat diets (HFD) modulate hippocampal neuroinflammation *in vivo* and explored target-level mechanisms with molecular docking. Male B6129SF2/J mice received a standard diet (SD) or HFD enriched with extra-virgin olive oil (EVOO), refined olive oil (ROO), refined palm oil (RPO), or ω3 long-chain polyunsaturated fatty acids (ω3-LCPUFA). During the final week, scopolamine induced acute cholinergic dysfunction. Neuroinflammation was assessed in the dentate gyrus by IHC (Iba-1, COX-2, and TNF-α) and by IF of astrocytes (GFAP intensity and morphology). Docking was employed to evaluate interactions of oleic and palmitic acids, EPA, and DHA with AChE, COX-2, BACE1, and TREM2. All HFD groups attenuated scopolamine-induced increases in Iba-1, COX-2 and TNF-α compared with the SD-scopolamine group, with limited separation among lipid classes under this acute stressor. By contrast, astroglial readouts showed a clear hierarchy: EVOO-HFD produced the lowest GFAP signal and the most ramified morphology, followed closely by ω3-LCPUFA, with ROO being intermediate and SFA being the least favourable. Docking supported a mechanistic framework: EPA/DHA displayed stronger predicted engagement than oleate/palmitate at COX-2 and BACE1, while long-chain fatty acids occupied the AChE peripheral site and a lipid/apoE-responsive surface on TREM2. In conclusion, PUFA-rich feeding, and notably that with the EVOO matrix, preferentially buffers hippocampal neuroinflammation in a scopolamine-induced Alzheimer's-like model. These findings support a composition, binding, and function framework and strengthen the translational rationale for precision nutrition strategies prioritizing ω3-LCPUFA and high-quality olive oils.

Received 19th January 2026,
Accepted 10th April 2026

DOI: 10.1039/d6fo00279j

rsc.li/food-function

Open Access Article. Published on 17 April 2026. Downloaded on 5/30/2026 11:00:16 AM.
This article is licensed under a Creative Commons Attribution-NonCommercial 3.0 Unported Licence.

1. Introduction

Alzheimer's disease (AD) is a multifactorial neurodegenerative disorder in which amyloid-β (Aβ) deposition and tau pathology coexist with a persistent, maladaptive neuroinflammatory milieu orchestrated by microglia and astrocytes.[1] Beyond the classical proteinopathies, disturbances in lipid handling and membrane composition are increasingly recognised as upstream drivers of immune dysregulation and synaptic failure, placing brain lipid metabolism and its dietary determinants at the centre of disease biology.[2,3]

Diet quality, particularly the fatty acid profile and the presence of bioactive phenolics from olive products, has been consistently linked to brain health.[4,5] Adherence to Mediterranean-style dietary patterns, characterised by extra-virgin olive oil (EVOO) as the principal fat source, is associated with more favourable cognitive trajectories, whereas Western-type fat patterns enriched in saturated fatty acids (SFAs) align with neuroinflammatory phenotypes.[6,7] Mechanistically, EVOO phenolics and the broader food matrix modulate oxidative and inflammatory pathways and engage the gut–brain axis, providing a plausible route by which specific foods can reshape neuroinflammatory and immune responses in the brain.[8] Among dietary fats, omega-3 long-chain polyunsaturated fatty acids (ω3-LCPUFAs), such as docosahexaenoic acid (DHA) and eico-

[a]*Department of Medical Biochemistry, Molecular Biology and Immunology, School of Medicine, University of Seville, Av. Sanchez Pizjuan s/n, 41009 Seville, Spain*
[b]*Instituto de Biomedicina de Sevilla, IBiS/Hospital Universitario Virgen del Rocio/CSIC/Universidad de Sevilla, Seville, 41013, Spain*
[c]*Department of Pharmacology, Pediatrics, and Radiology, School of Medicine, University of Seville, 41009 Seville, Spain. E-mail: cmclaro@us.es*

Open Access Article. Published on 17 April 2026. Downloaded on 5/30/2026 11:00:16 AM.
This article is licensed under a Creative Commons Attribution-NonCommercial 3.0 Unported Licence.

sapentaenoic acid (EPA), exert neuroprotective actions that include modulating microglial phenotype and function.[9] Experimental and translational evidence indicate that ω3-LCPUFAs availability shapes microglial lipid metabolism and phagocytic programmes, whereas deficiency states exacerbate synaptic pruning and behavioural impairment.[10,11] These data converge on the principle that brain-resident immunity is exquisitely sensitive to systemic lipid inputs. In parallel, olive-derived phenolics interact with AD-relevant pathways.[12] Oleocanthal enhances Aβ clearance and reduces aggregation toxicity, supporting a food-borne small-molecule rationale alongside macronutrient effects, while broader EVOO phenolic profiles display antioxidant and anti-inflammatory activities pertinent to neurodegeneration.[13,14] Together, these strands point to the complementary, multi-tiered benefits of both fatty acid quality and phenolic biochemistry within olive-centred dietary patterns. At the same time, not all fatty acids are equal. SFAs such as palmitic acid have been reported to promote inflammatory signalling, including proposed TLR4/MD-2 interactions; however, this remains debated and may reflect broader lipid-induced immunometabolic reprogramming rather than direct receptor ligation.[15–17] These mixed findings underscore the need to resolve lipid–protein interaction landscapes relevant to neuroinflammation. Molecular docking, therefore, provides a tractable first pass to map how major dietary fatty acids might engage AD- and inflammation-related targets, complementing *in vivo* models that test causal links between dietary fat quality and neuroimmune outcomes.[18]

Herein, building on this framework, we investigate whether dietary fat quality modulates neuroinflammatory readouts in a murine model of AD-like cholinergic dysfunction and, in parallel, we perform *in silico* docking of the major fatty acids from each diet against canonical AD/neuroinflammatory targets to propose mechanistic links between nutrient composition and neuroimmune signalling. This integrated strategy is designed to connect composition, binding, and function, thereby strengthening the translational rationale for precision nutrition approaches in Alzheimer's-relevant contexts.

2. Materials and methods

2.1. Materials

Unless otherwise specified, analytical-grade reagents were used. Dietary lipid sources for diet preparation and lipid profiling include extra-virgin olive oil (EVOO) and refined olive oil (ROO; Ybarra, Seville, Spain), refined palm oil (RPO; LIPSA, Barcelona, Spain), and fish-oil capsules (Omacor®, Seville, Spain). Primary antibodies were anti-Iba-1 (rabbit, 1 : 500; Santa Cruz, Dallas, TX, USA, sc-98468), anti-COX-2 (goat, 1 : 200; Santa Cruz, sc-1747), anti-TNF-α (mouse, 1 : 100; Santa Cruz, sc-133192), and anti-GFAP (rabbit, 1 : 500; Dako, Glostrup, Denmark, Z0334). Secondary antibodies (Vector Laboratories, Newark, CA, USA) were anti-rabbit IgG (HRP, 1 : 1000; BA-1000), anti-goat IgG (HRP, 1 : 500; BA-5000), and anti-mouse IgG (HRP, 1 : 500; BA-2000). For immunofluorescence (IF), FITC-conjugated anti-rabbit IgG was used (1 : 500; Jackson, West Grove, PA, USA, 711-095-152). Chromogenic detection employed DAB (Sigma-Aldrich, Darmstadt, Germany) and the ABC kit (Vector, PK-6100). Nuclear counterstaining used Hoechst/DAPI, and neurodegeneration was assessed with the Fluoro-Jade C kit (FJC, Biosensis, Thebarton, SA, Australia), following manufacturer instructions. Imaging was performed on an Olympus BX41 microscope with an XM10 camera (Olympus, Tokyo, Japan) and on a Zeiss LSM 7 DUO confocal system (Carl Zeiss, Oberkochen, Germany); image analysis was conducted in ImageJ (NIH, Bethesda, MD, USA) under identical acquisition settings across groups.

2.2. Fatty acid profiling of oils (GC-FID)

Fatty-acid methyl esters (FAMEs) were analysed on a GC 6890N equipped with a flame-ionization detector (FID, Agilent Technologies, Santa Clara, CA, USA) using an HP-88 capillary column (100 m × 0.25 mm i.d., 0.2 μm film; Agilent J&W, Folsom, CA, USA).[19] The carrier gas was hydrogen at 2 mL min^{-1} (constant-flow mode). The oven programme was as follows: 100 °C (start), ramp 3 °C min^{-1} to 158 °C, then 1.5 °C min^{-1} to 190 °C (hold 15 min), then 2 °C min^{-1} to 200 °C, then 10 °C min^{-1} to 240 °C (hold 10 min). Injector: 300 °C; detector: 320 °C. Peaks were identified against a certified FAME standard mixture, and results are expressed as g per 100 g of total fatty acids (SI Table S1).

2.3. Animals, ethics, diets, and experimental design

Male B6129SF2/J mice (5–8 weeks; The Jackson Laboratory, Bar Harbor, ME, USA, stock 101045) were housed (2–4 per cage) under a 12 h light/dark cycle at 21 ± 2 °C and 50%–50% relative humidity, with *ad libitum* access to water and chow and standard environmental enrichment. All procedures complied with EU Directive 2010/63 and Spanish RD 53/2013 and were approved by the Animal Research Ethics Committee of the University of Seville and the Andalusian Committee for Animal Experimentation (approval 26/08/2020/101). After 1 week of acclimatization, mice were randomized into five dietary groups (n = 8–10 per group): (i) SD (standard diet); (ii) HFD-MUFA (SD supplemented with 47% EVOO); (iii) HFD-rMUFA (47% ROO); (iv) HFD-SFA (47% RPO); and (v) HFD-ω3-LCPUFA (32% ROO + 15% fish oil). The supplementation level (47%) was selected to convert the standard chow (≈13% energy from fat) into a high-fat dietary background providing ~60% of total energy from fat, thereby creating an obesogenic/metabolic-stress context in which fat quality (source and fatty-acid profile) could be tested while keeping the overall fat-derived energy comparable across high-fat groups (13% from chow + 47% from supplemented oils). Thus, the study design was isocaloric/isofat across HFD groups, differing primarily in the lipid source and fatty-acid composition. For the HFD-ω3-LCPUFA group, the total supplemented oil was kept constant (47%) to maintain comparable fat-derived energy; however, 15% of the supplemented lipid was provided as fish oil to enrich the diet in EPA/DHA, while the remaining 32% ROO served as a MUFA background/carrier to preserve diet comparability and feasibility and to

 This journal is © The Royal Society of Chemistry 2026

Open Access Article. Published on 17 April 2026. Downloaded on 5/30/2026 11:00:16 AM.
This article is licensed under a Creative Commons Attribution-NonCommercial 3.0 Unported Licence.

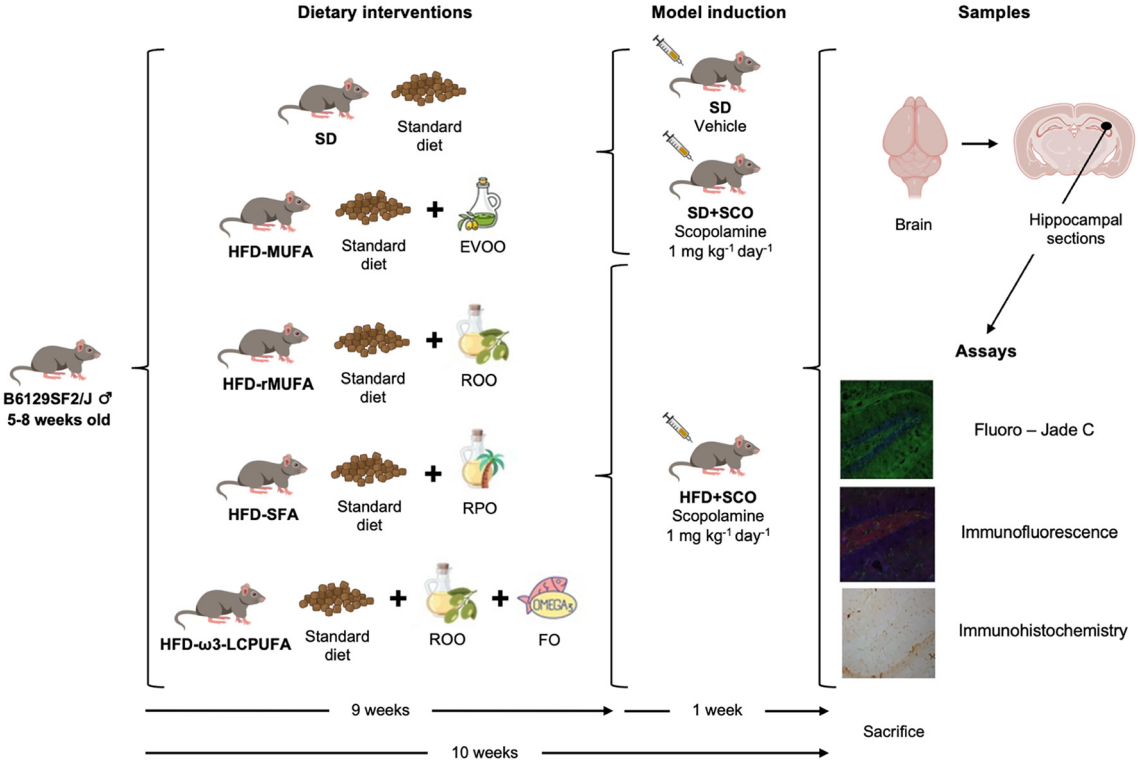

Fig. 1 Schematic of the 10 week feeding intervention and scopolamine challenge. After a 1 week acclimatization, male B6129SF2/J mice were randomized to standard diet (SD), HFD-MUFA (extra-virgin olive oil, EVOO), HFD-rMUFA (refined olive oil, ROO), HFD-SFA (refined palm oil, RPO), or HFD-ω3-LCPUFA (ROO + fish oil, FO). Scopolamine (1 mg kg^{-1}, i.p.) was administered on three alternating days during the final week to all groups except one SD subgroup (vehicle control). Body weight and food intake were recorded weekly. At week 10, brains were collected for IHC/IF and Fluoro-Jade C analyses. All outcome assessments and image quantifications were performed by investigators unaware of the experimental group allocation.

avoid using fish oil as the sole supplemental fat (which can be more prone to oxidation and may impact palatability and intake). Body weight and food intake were recorded weekly. During the final week, all groups, except half of the SD group, received scopolamine hydrobromide (1 mg kg^{-1}, i.p.; three injections on alternating days over 5 days) to induce Alzheimer's-like cholinergic dysfunction;[20] the remaining SD subgroup received vehicle and served as an intra-group control. At week 10, animals were anesthetised (ketamine 100 mg kg^{-1} + xylazine 10 mg kg^{-1}, i.p.) and euthanised; brains were collected for histological analyses. Outcome assessment and image quantification were performed blinded to group allocation. A schematic of the experimental timeline and group allocation is shown in Fig. 1.

2.4. Tissue processing and histological analyses

Brains were immersion-fixed in 10% paraformaldehyde for 24 h, cryoprotected in 15% and then 30% sucrose, embedded in OCT, and stored at −80 °C. Coronal sections (hemisphere, 20 μm) were cut at −20 °C and collected in PBS/glycerol (50%) for downstream immunohistochemistry (IHC), IF, or FJC staining. For IHC, hippocampal sections were washed in PBS, endogenous peroxidase was quenched with H_2O_2, and non-specific binding was blocked with 10% FBS. Sections were incubated for 24 h at 4 °C with primary antibodies (Iba-1, 1 : 500; COX-2, 1 : 200; TNF-α, 1 : 100) diluted in PBS-T + 3% FBS, washed, and incubated with the corresponding HRP-conjugated secondary antibodies (anti-rabbit 1 : 1000 for Iba-1; anti-goat 1 : 500 for COX-2; anti-mouse 1 : 500 for TNF-α). Signal was developed using ABC and DAB; sections were dehydrated, cleared, mounted with DPX, and imaged under identical acquisition settings across groups. For IF (astroglial markers), sections were permeabilised in PBS-T (1%), blocked with BSA (5%), and incubated overnight at 4 °C with anti-GFAP (1 : 500) in PBS-T + 1% BSA. After washing, sections were incubated for 1 h at room temperature in the dark with FITC-conjugated anti-rabbit IgG (1 : 500); Hoechst/DAPI was added during the last 5 min for nuclear counterstaining. Sections were mounted and imaged by confocal microscopy. FJC staining to assess neurodegeneration followed the manufacturer's protocol: ethanol/NaOH pre-treatment, $KMnO_4$ background suppression, FJC/DAPI staining, dehydration, mounting, and confocal imaging with uniform settings. Image quantification was performed in ImageJ with constant thresholds and blinded analysis. For IHC, the positively stained area or integrated density for Iba-1, COX-2, and TNF-α was quantified in anatomically matched hippocampal regions (three sections per mouse). For IF-GFAP, integrated density, circularity ($4\pi \times$ area per perimeter^2), and aspect ratio (major axis/minor axis) were computed from binarised images to capture astrocyte reactivity

Open Access Article. Published on 17 April 2026. Downloaded on 5/30/2026 11:00:16 AM.
This article is licensed under a Creative Commons Attribution-NonCommercial 3.0 Unported Licence.

and morphology. For glial analyses, brain sections were selected using the same anatomical criteria across animals (comparable rostro–caudal levels) and processed in parallel to minimize batch effects. Images were acquired under identical microscope settings for all groups (exposure/gain/laser power kept constant within each marker). For each animal, multiple non-overlapping fields of view were recorded per section and across sections within the region(s) of interest, and the mean value per animal was used for all downstream statistical analyses (the animal as the experimental unit).

2.5. Molecular docking of major dietary fatty acids

We assessed putative interactions between prevalent dietary fatty acids and AD-related proteins using a standardised, structure-based docking workflow. Oleic acid (PubChem CID 445639), palmitic acid (985), EPA (445580), and DHA (5281168) were downloaded as SDF files, imported into UCSF Chimera v1.16, protonated at pH 7.4, assigned Gasteiger charges and energy-minimised; all ligand torsions were left flexible and PDBQT files were generated with MGLTools/AutoDockTools v1.5.7. Receptors were the TREM2 ectodomain (PDB 5UD7), acetylcholinesterase (AChE, 5DTI), COX-2 (PDB 1DDX), and β-secretase 1 (BACE1, 1FKN), retrieved from the RCSB PDB, inspected for missing residues/alternate conformers, stripped of co-ligands/ions/waters, protonated at pH 7.4, locally minimised in binding pockets when needed, and saved as PDBQT. Binding sites and grid maps were generated with AGFR (ADFR Suite v1.0): for AChE, COX-2, and BACE1, grids were centred on the orthosteric cavities defined by their co-crystallized ligands; for TREM2, the grid encompassed the ApoE-interacting surface previously implicated in agonist responses.[21] Grid boxes covered the pocket plus ~4–6 Å margins (grid spacing 0.375 Å). Docking was performed with AutoDockFR (ADFR Suite v1.0; AD4 scoring) under high-search settings (100 GA runs/ligand, population 200, $\sim 2.5 \times 10^6$ evaluations per run; random seed 12345). Receptors were rigid by default, and a sensitivity check allowed limited side-chain flexibility of the hydrophobic binding pocket. Quality control included redocking, accepting poses with RMSD $\leq$ 2.0 Å *versus* crystallographic poses. The best pose per ligand–target pair was selected by predicted binding free energy (ΔG, kcal mol^{-1}) and chemical plausibility and analysed in BIOVIA Discovery Studio Visualizer v21 to generate 2D/3D interaction summaries.

2.6. Statistical analysis

Data are reported as mean ± SD, with the animal as the unit of analysis (n = 8–10 per group). Group comparisons were performed by one-way ANOVA followed by Tukey's *post hoc* test. Statistical significance was set at $p < 0.05$. We have reported exact p-values (to four decimals, or "$p < 0.001$"). Analyses and plots were generated in GraphPad Prism v10.4.2 (GraphPad Software, San Diego, CA, USA). All quantifications were conducted blinded to group allocation. The animal was considered the independent biological replicate. Although multiple sections and fields of view were analysed per animal, these measurements were used solely to obtain a robust animal-level mean; they were not treated as independent observations (*i.e.*, no pseudoreplication). Accordingly, all statistical comparisons were performed using animal-level summary values.

3. Results and discussion

3.1. Dietary fat quality diverges body weight trajectories and modulates acute neurodegeneration

Across the 10 week intervention, body mass diverged as a function of fat quality (SI Fig. S1). The HFD-SFA produced the largest gain (≈ >30%), HFD-rMUFA an intermediate profile (≈25%), whereas the HFD-ω3-LCPUFA blunted weight gain toward standard chow values (≈11%; p = 0.0412, HFD-ω3-LCPUFA *vs.* HFD-SFA). HFD-MUFA (EVOO) tended to attenuate accrual *versus* refined MUFA despite broadly similar fatty-acid classes, consistent with matrix/phenolic co-factors lost upon refining. Although several contrasts did not reach significance, the directionality supports a role for processing and matrix, not only fatty acid class, in energy balance. During the scopolamine week, HFD groups showed partial weight recovery, whereas SD-Sco displayed a more persistent loss, suggesting short-term metabolic buffering under acute cholinergic stress. This systemic context is relevant because energetic status, adipokines, and steroid milieu can shape neurodegenerative susceptibility.

FJC staining in the dentate gyrus revealed a diet-sensitive neurodegenerative response to scopolamine (Fig. 2). SD-Sco displayed a higher FJC-positive signal than SD (p = 0.0141), indicating increased neuronal vulnerability under acute cholinergic blockade. High-fat feeding modulated this response with a clear quality hierarchy: HFD-MUFA (EVOO) exhibited the lowest FJC burden among HFDs (p = 0.0246 *vs.* SD-Sco), HFD-ω3-LCPUFA was similarly low, HFD-rMUFA was intermediate, and HFD-SFA trended highest. These patterns are consistent with the hypothesis that PUFA richness and the EVOO matrix, which adds bioactive phenolics absent in ROO, confer resilience to acute neurodegenerative stress, whereas an SFA-biased milieu is less favourable.[6] Several non-exclusive mechanisms may account for these differences: biophysical membrane effects, where ω3 chains enhance fluidity and may reduce susceptibility to calcium dysregulation and excitotoxic cascades;[22,23] redox/inflammatory buffering *via* endogenous lipid mediators derived from ω3 substrates and phenolic antioxidants present in EVOO;[24] and metabolic preconditioning, whereby differences in weight trajectory and systemic milieu (*e.g.*, adipokines, glucocorticoids) alter the brain's threshold to acute injury.[25] Accordingly, the ω3-LCPUFA arm should be interpreted as EPA/DHA enrichment within a MUFA-rich dietary context rather than as the effect of fish oil alone. This formulation is not expected to compromise ω3 bioavailability and may improve dietary stability and comparability among groups. The relative advantage of EVOO over refined MUFA suggests that food matrix components can amplify benefits beyond oleate content. Two considerations temper interpretation. First, FJC identifies ongoing degeneration but does not specify death pathways; pairing FJC with neuronal markers (*e.g.*, NeuN) and apoptosis/oxidative readouts would refine attribu-

This journal is © The Royal Society of Chemistry 2026

Open Access Article. Published on 17 April 2026. Downloaded on 5/30/2026 11:00:16 AM.
This article is licensed under a Creative Commons Attribution-NonCommercial 3.0 Unported Licence.

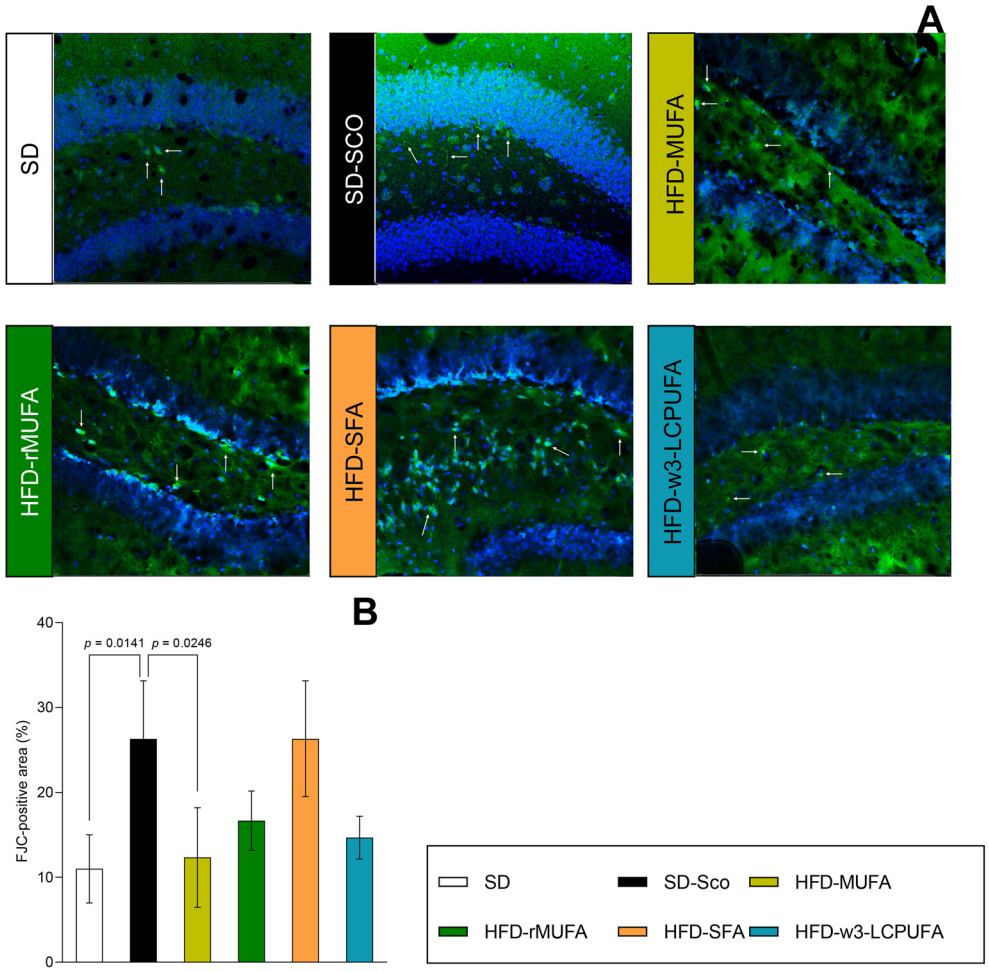

Fig. 2 Fluoro-Jade C identifies scopolamine-induced neurodegeneration with diet-dependent modulation in the dentate gyrus. (A) Representative FJC/DAPI micrographs (arrows highlight FJC-positive degenerating profiles) and (B) quantification across SD, SD-Sco, HFD-MUFA (EVOO), HFD-rMUFA (ROO), HFD-SFA (RPO), and HFD-ω3-LCPUFA. Scopolamine increased FJC-positive signal relative to SD, whereas ω3-LCPUFA and EVOO showed the lowest values among HFDs, with SFA tending higher; exact *p*-values for significant contrasts are reported on the plot. Quantification was performed blinded on anatomically matched dentate-gyrus ROIs (three sections per mouse; n = 3–4 mice per group) under identical acquisition settings. *Y*-axis: FJC-positive area (%).

tion. Second, the scopolamine window is short and high-amplitude; extending dietary exposure, lengthening the post-challenge interval, and increasing group size would improve sensitivity to resolve differences between MUFA sources and to determine whether SFA-associated vulnerability persists or escalates.[26] Even with these boundaries, the convergence of body-weight patterns and FJC burden supports the conclusion that dietary fat quality and matrix shape systemic status and buffer acute neurodegeneration, with EVOO showing the most favourable profile and ω3-LCPUFA a close second.

3.2. Microglial activation and inflammatory effectors are dampened by HFDs but show limited separation across lipid classes under scopolamine stress

In the dentate gyrus, scopolamine elicited the expected inflammatory surge, with higher densities of Iba-1+, TNF-α+ and COX-2+ profiles in SD-Sco *versus* SD, consistent with a rapid shift toward a reactive microglial milieu under acute cholinergic stress (Fig. 3, representative TNF-α and COX-2 micrographs in SI Fig. S2–S3). Across all HFDs, this increase was significantly blunted relative to SD-Sco, bringing all three markers closer to SD values; however, pairwise contrasts among HFDs were not significant (one-way ANOVA/Tukey), indicating that in this short, high-amplitude window, dominant high-fat exposure effects override finer distinctions attributable to fatty acid class. At the marker level, Iba-1 reductions indicate fewer microglia in an activated state; although Iba-1 is not state-exclusive, it remains a widely used readout of microglial presence/reactivity in brain tissue.[27] Lower TNF-α is aligned with curtailed cytokine signalling that perturbs synaptic function and plasticity during neuroinflammation, offering a parsimonious explanation for the attenuated effector milieu in HFD groups.[28] The decline in COX-2 is compatible with damping of the eicosanoid/oxidative arm of the response in the hippocampus, where COX-2 activity influences neuronal excitability and network dynamics.[29] The con-

Open Access Article. Published on 17 April 2026. Downloaded on 5/30/2026 11:00:16 AM.
This article is licensed under a Creative Commons Attribution-NonCommercial 3.0 Unported Licence.

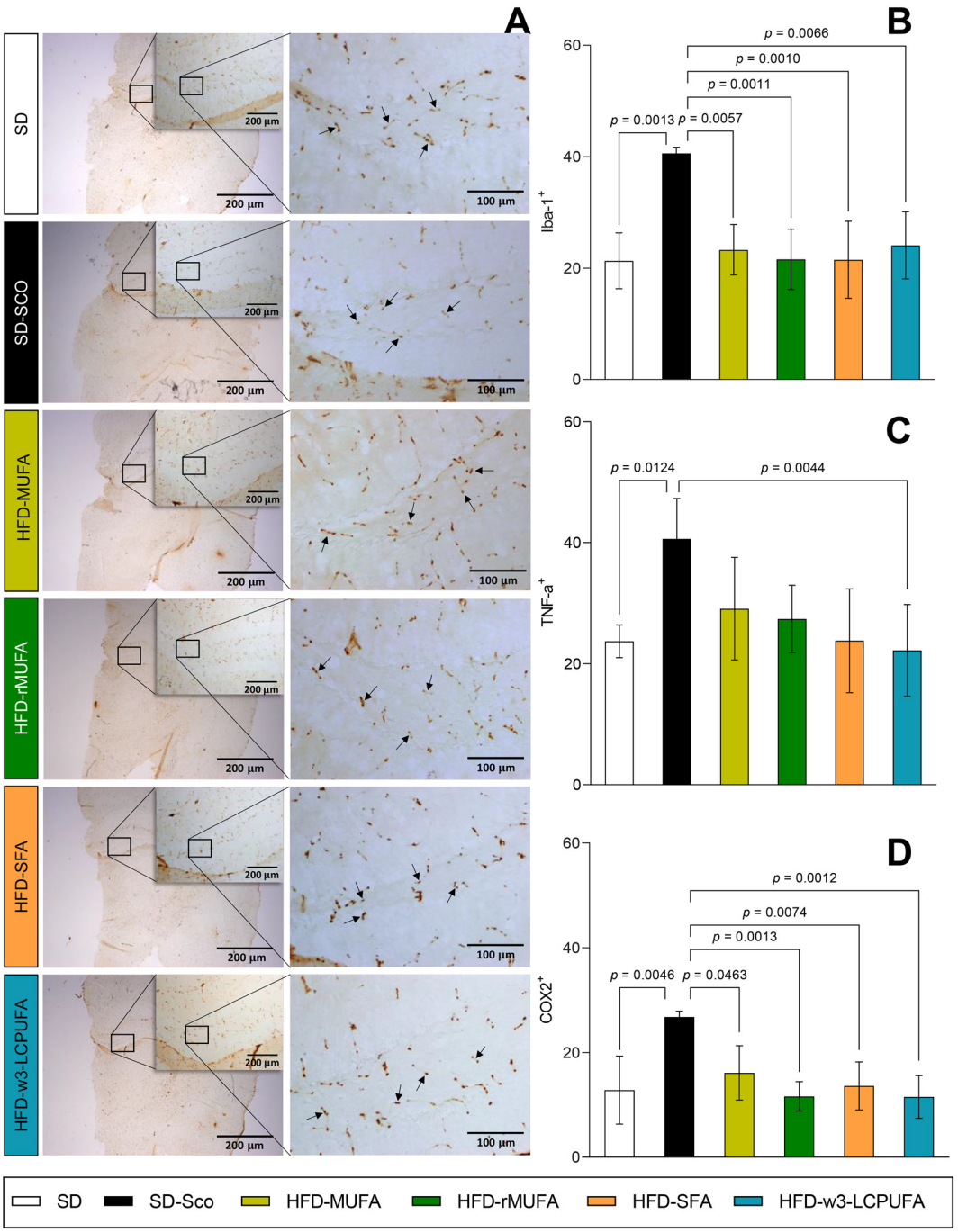

Fig. 3 High-fat diets attenuate scopolamine-induced microglial and inflammatory markers in the dentate gyrus. (A) Representative IHC micrographs (left; low-magnification overview with inset; right: high-magnification ROI), and quantification for (B) Iba-1, (C) TNF-α, and (D) COX-2 across SD, SD-Sco, HFD-MUFA (EVOO), HFD-rMUFA (ROO), HFD-SFA (RPO), and HFD-ω3-LCPUFA. Arrows indicate representative Iba-1-positive profiles within the dentate gyrus (brown DAB signal). Quantification was performed blinded on anatomically matched dentate gyrus sections (three sections per mouse). Data are mean ± SD; one-way ANOVA with Tukey's *post hoc* test. Exact *p*-values for significant contrasts are reported on the plots. Scale bars: 200 µm (overview) and 100 µm (insets).

cordant directionality across these independent readouts argues for a coordinated dampening rather than assay-specific variance or thresholding artefacts and is supported by identical acquisition settings and blinded quantification in matched hippocampal sections. Mechanistically, the absence of separation among HFD classes under acute scopolamine likely reflects compression of between-group variance by a brief, high-amplitude insult, together with the inherently coarse granularity of density-based IHC markers for detecting second-order lipid-class effects. Extending the dietary exposure and

Open Access Article. Published on 17 April 2026. Downloaded on 5/30/2026 11:00:16 AM.
This article is licensed under a Creative Commons Attribution-NonCommercial 3.0 Unported Licence.

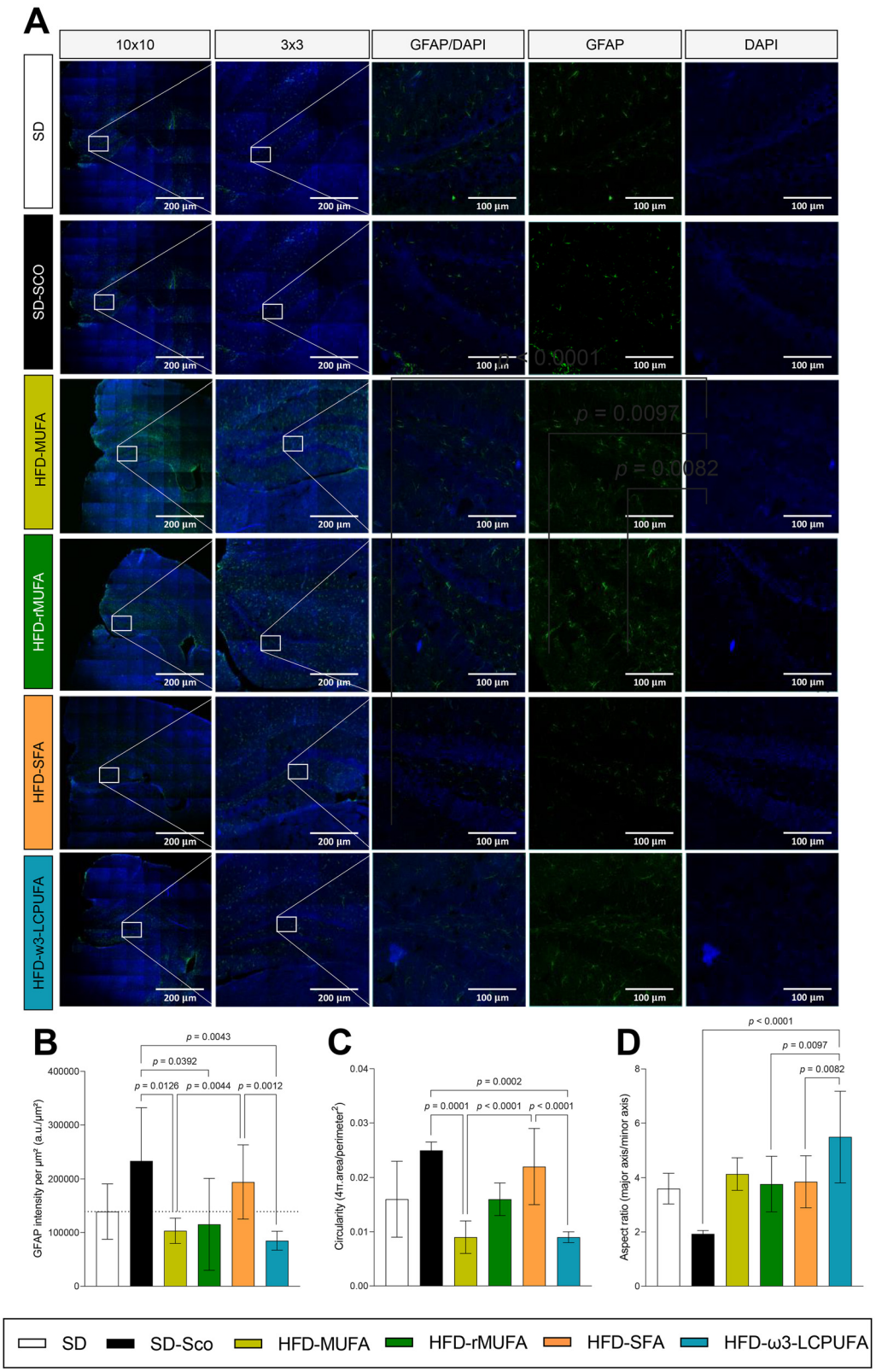

Fig. 4 Astrocyte reactivity is diet-dependent under scopolamine. (A) Representative confocal images of the dentate gyrus (columns: 10 × 10 overview, 3 × 3 zoom, GFAP/DAPI merge, GFAP channel, and DAPI channel) and (B) quantification of GFAP intensity per µm^2 (a.u. µm^{-2}), (C) circularity (4π × area per perimeter^2), and (D) aspect ratio (major axis/minor axis) across SD, SD-Sco, HFD-MUFA (EVOO), HFD-rMUFA (ROO), HFD-SFA (RPO), and HFD-ω3-LCPUFA. Scopolamine increased GFAP intensity and drove hypertrophic, less-elongated astrocytes (higher circularity and lower aspect ratio) relative to SD. All HFDs mitigated this response, with ω3-LCPUFA showing the lowest GFAP signal and most favourable morphology, followed by EVOO, then rMUFA, and SFA. Exact *p*-values for significant contrasts are shown on the plots. Imaging was performed under identical acquisition settings; quantification was blinded on anatomically matched sections (three sections per mouse). Scale bars: 200 µm (overview) and 100 µm (zoom and single-channel panels).

Open Access Article. Published on 17 April 2026. Downloaded on 5/30/2026 11:00:16 AM.
This article is licensed under a Creative Commons Attribution-NonCommercial 3.0 Unported Licence.

the post-challenge interval, and increasing group size, particularly for histological endpoints, are recommended to resolve subtler differences between MUFA sources and to determine whether SFA-associated vulnerability persists or escalates in longer windows of observation.

Although pairwise contrasts among HFDs did not reach significance, the bar patterns consistently suggest ω3-LCPUFA at or near the lowest inflammatory values, with EVOO frequently trending below ROO and SFA. Two features likely obscured class effects. First, acute scopolamine delivers a steep, rapidly resolving neuroimmune pulse that can compress variance and floor between-diet differences once any HFD is present.[26] Second, density-based IHC metrics (Iba-1/COX-2/TNF-α), while appropriate for detecting large state shifts, are intrinsically less sensitive than morphology-aware descriptors (*e.g.*, process complexity, convex hull, nearest-neighbour spacing) for capturing lipid-class influences.[30] This reading is congruent with our astroglial IF, where GFAP intensity and shape descriptors show a clearer gradient (ω3-LCPUFA > EVOO-MUFA ≳ rMUFA > SFA), implying that astrocytes are earlier or more sensitive integrators of dietary lipid cues, whereas microglia display a shared buffering under the present acute paradigm. Mechanistically, several non-exclusive routes could account for the HFD-wide attenuation. Systemically, high-fat feeding remodels endocrine and adipokine profiles and stress physiology, potentially resetting brain immune set-points before the cholinergic challenge.[31] At the cellular level, even short exposures can recompense membrane lipids and raft architecture, adjusting receptor thresholds and signalling gain; such rapid remodelling would favour a class-agnostic reduction when the insult is brief.[32] In parallel, gut–brain communication, including microbial metabolites and vagal inputs, may converge on hippocampal microglia to limit peak responses.[33] While our design does not disentangle these pathways, the internal consistency across markers supports a shared upstream influence during the scopolamine window. Importantly, the docking layer provides target-level plausibility for quality-dependent effects that may require longer exposure or progressive pathology to become histologically apparent: EPA/DHA showed the most favourable engagement at COX-2 and BACE1, and long-chain fatty acids occupied the AChE peripheral site and a TREM2 lipid/apoE-responsive interface, outlining biochemical routes by which ω3-rich or EVOO-based diets could differentially modulate eicosanoid, amyloidogenic, cholinergic and microglial-sensing axes, even if such separations do not yet reach significance among HFDs in this acute model. Together, these considerations support a two-tier interpretation: a broad, short-term buffering of scopolamine-induced microglial activation common to all HFDs that collapses between-diet differences in Iba-1/COX-2/TNF-α densities; and diet-quality–sensitive modulation that emerges more clearly in astrocyte metrics and is foreshadowed by *in silico* target engagement. To increase microglial resolution, future studies should increase histological sample sizes, extend the dietary intervention and post-challenge windows, incorporate morphology- and spatially aware microglial analytics, and pair histology with hippocampal lipid-mediator profiling (COX-2-linked prostanoids and specialised pro-resolving mediators) to test whether the predicted docking hierarchy is mirrored by shifts in the eicosanoid networks.

3.3. Astrocyte reactivity tracks dietary fat quality and aligns with omega-3 enrichment and EVOO matrix effects

IF for GFAP in the dentate gyrus revealed a clear, diet-dependent modulation of astrocyte reactivity under scopolamine (Fig. 4). Relative to SD, SD-Sco showed higher GFAP intensity and a shift toward a hypertrophic morphology, greater circularity and lower aspect ratio, consistent with swollen, less ramified astrocytes. All HFDs reduced this response to some extent, but the magnitude followed a consistent hierarchy. HFD-ω3-LCPUFA displayed the lowest GFAP signal among HFDs (p = 0.0043 *vs.* HFD-SFA) and the most favourable morphology (reduced circularity, $p < 0.0001$; increased aspect ratio, p = 0.0082; both *vs.* HFD-SFA), with HFD-MUFA (EVOO) as a close second. HFD-rMUFA occupied an intermediate position, whereas HFD-SFA showed the smallest improvement and frequently remained closest to SD-Sco. Taken together, the gradient ω3-LCPUFA > EVOO > rMUFA > SFA across three orthogonal GFAP metrics (integrated intensity per area, circularity, and aspect ratio) supports the view that fat quality, and, specifically, omega-3 enrichment and the EVOO matrix, meaningfully modulate astrocyte state during an acute cholinergic challenge. Several non-exclusive factors could account for this pattern. First, lipid class-dependent membrane remodelling may influence astrocytic calcium dynamics,[34] gap-junction coupling,[35] and susceptibility to oxidative stress,[36] with long-chain ω3 chains favouring a more compliant bilayer than SFA-rich profiles. Second, bioactive phenolics present in EVOO but largely absent from refined oils can provide additional antioxidant and anti-inflammatory buffering, either directly within astrocytes or indirectly *via* the perivascular niche, facilitating restoration of a more ramified/physiologic morphology.[37] Third, diet-driven systemic cues (energy balance, adipokines, stress hormones) plausibly shift astroglial set-points and thereby alter the magnitude of the acute response

Table 1 Predicted binding free energies (ΔG, kcal mol^{-1}) for dietary fatty acids docked to AChE, TREM2, BACE1, and COX-2. Values correspond to the best-scoring pose per complex; more negative values indicate stronger predicted binding

	Ligand			
Target	Palmitic acid (C16:0)	Oleic acid (C18:1ω9)	EPA (C20:5ω3)	DHA (C22:6ω3)
AChE	−6.5	−5.9	−7.6	−7.4
TREM2	−7.7	−7.7	−8.0	−7.4
BACE1	−6.8	−6.9	−8.4	−8.5
COX-2	−8.3	−9.2	−9.8	−10.5

AChE, acetylcholinesterase; BACE1, β-site APP cleaving enzyme 1; COX-2, cyclooxygenase-2; TREM2, triggering receptor expressed on myeloid cells 2; EPA, eicosapentaenoic acid; and DHA, docosahexaenoic acid.

 This journal is © The Royal Society of Chemistry 2026

Open Access Article. Published on 17 April 2026. Downloaded on 5/30/2026 11:00:16 AM.
This article is licensed under a Creative Commons Attribution-NonCommercial 3.0 Unported Licence.

to scopolamine.[25] Methodologically, the convergence of intensity and morphology metrics, together with uniform acquisition parameters and blinded quantification on matched sections, argues against threshold artefacts and supports a genuine biological separation among diets. The present readouts capture structural reactivity (GFAP load and shape descriptors) rather than pathway specificity; pairing morphology with indices of astrocytic metabolism (*e.g.*, glutamate

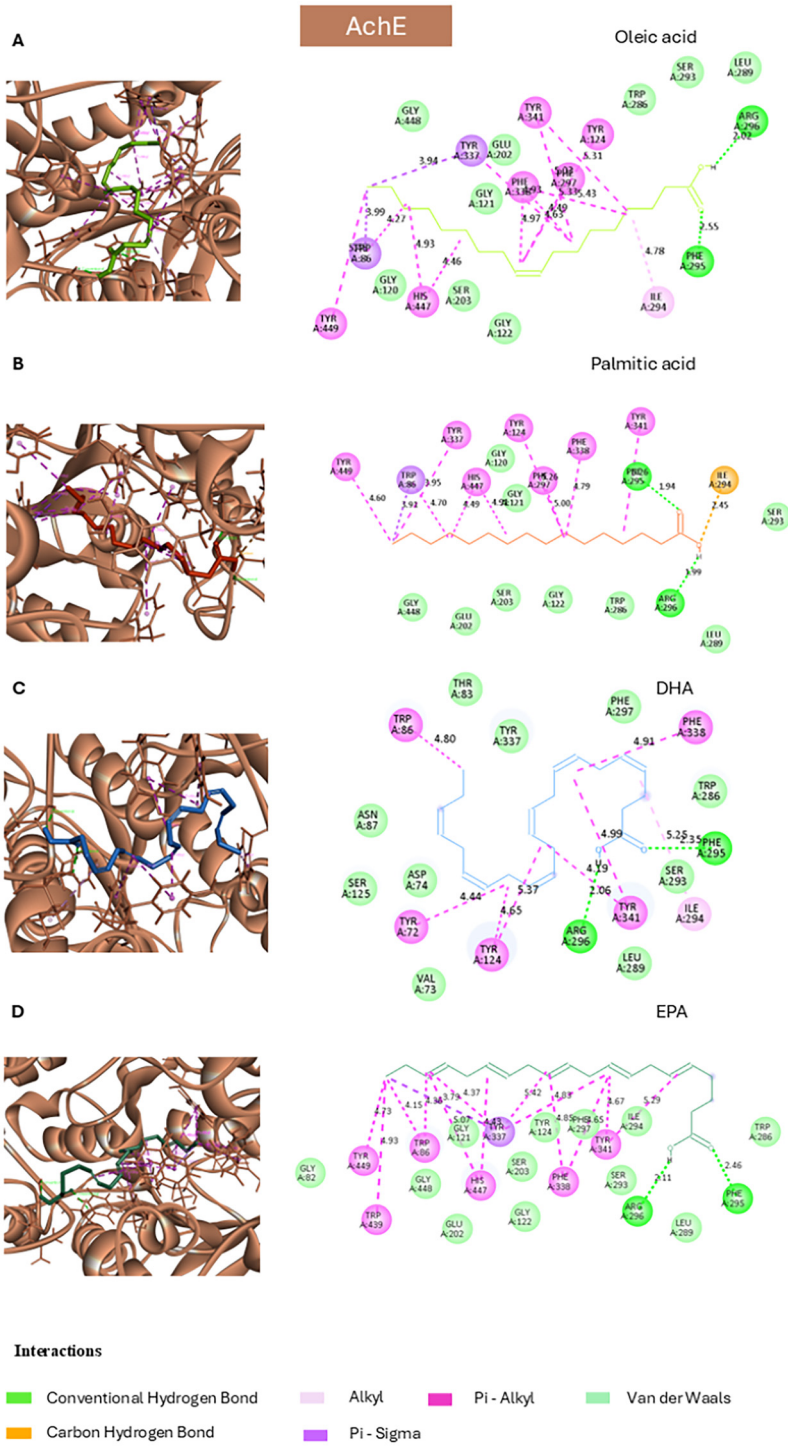

Fig. 5 Binding poses and interaction fingerprints of dietary fatty acids in the acetylcholinesterase (AChE; PDB 5DTI) active-site gorge. Left panels: best-scoring docked poses within the AChE binding gorge. Right panels: corresponding 2D interaction diagrams (hydrogen bonds, π/alkyl contacts, and van der Waals) generated in BIOVIA Discovery Studio Visualizer. (A) Oleic acid–AChE; (B) palmitic acid–AChE; (C) DHA–AChE; (D) EPA–AChE. Poses predominantly occupy the peripheral anionic site (PAS) region, with occasional proximity to the catalytic triad (Ser203–His447–Glu334), consistent with PAS-biased engagement rather than direct catalytic geometry. All images were produced using identical visualization settings.

Open Access Article. Published on 17 April 2026. Downloaded on 5/30/2026 11:00:16 AM.
This article is licensed under a Creative Commons Attribution-NonCommercial 3.0 Unported Licence.

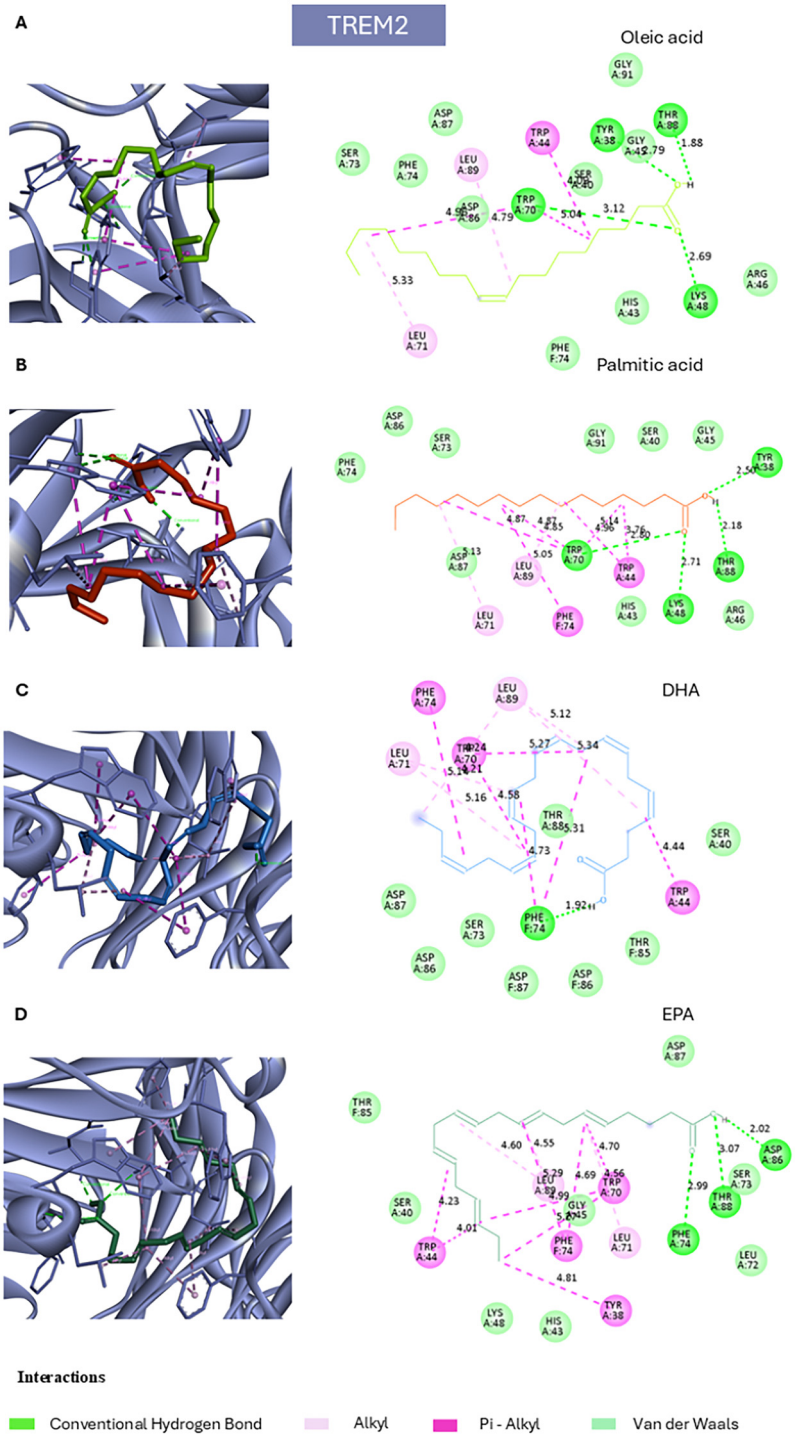

Fig. 6 Binding poses and interaction fingerprints of dietary fatty acids at the TREM2 (PDB 5UD7) ectodomain surface. Left panels: best-scoring docked poses on the apoE-interacting, agonist-responsive interface of TREM2. Right panels: corresponding 2D interaction diagrams (hydrogen bonds, π/alkyl and alkyl contacts, and van der Waals) generated in BIOVIA Discovery Studio Visualizer. (A) Oleic acid–TREM2; (B) palmitic acid–TREM2; (C) DHA–TREM2; (D) EPA–TREM2. Top-ranked poses consistently occupy the lipid/apoE-responsive surface; specific Arg47 salt bridges were not observed in the best poses, but engagement of the same functional patch supports a putative allosteric stabilization of TREM2 signalling. All renderings used identical visualization parameters.

This journal is © The Royal Society of Chemistry 2026

Open Access Article. Published on 17 April 2026. Downloaded on 5/30/2026 11:00:16 AM.
This article is licensed under a Creative Commons Attribution-NonCommercial 3.0 Unported Licence.

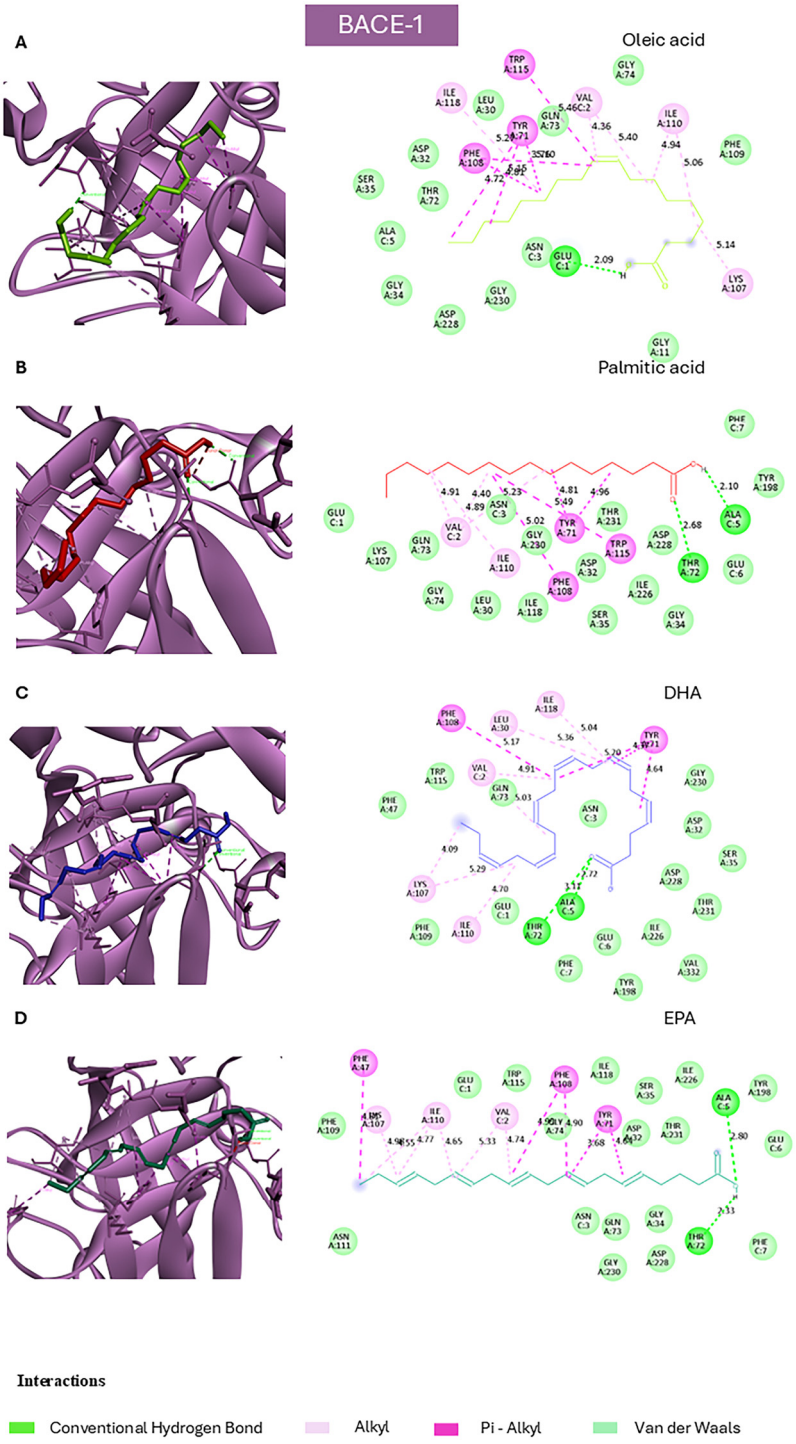

Fig. 7 Binding poses and interaction fingerprints of dietary fatty acids in the β-secretase 1 (BACE1; PDB 1FKN) catalytic cleft. Left panels: best-scoring docked poses within the active site of BACE1. Right panels: corresponding 2D interaction diagrams (hydrogen bonds, π/alkyl and alkyl contacts, and van der Waals) generated in BIOVIA Discovery Studio Visualizer. (A) Oleic acid–BACE1; (B) palmitic acid–BACE1; (C) DHA–BACE1; (D) EPA–BACE1. Poses occupy the catalytic cleft with predominant contacts to lining residues (*e.g.*, Thr72 and Phe108) and mainly van der Waals proximity to the Asp32–Asp228 catalytic dyad, consistent with substrate-gating/micro-allosteric engagement rather than tight competitive inhibition. All renderings used identical visualization parameters.

Open Access Article. Published on 17 April 2026. Downloaded on 5/30/2026 11:00:16 AM.
This article is licensed under a Creative Commons Attribution-NonCommercial 3.0 Unported Licence.

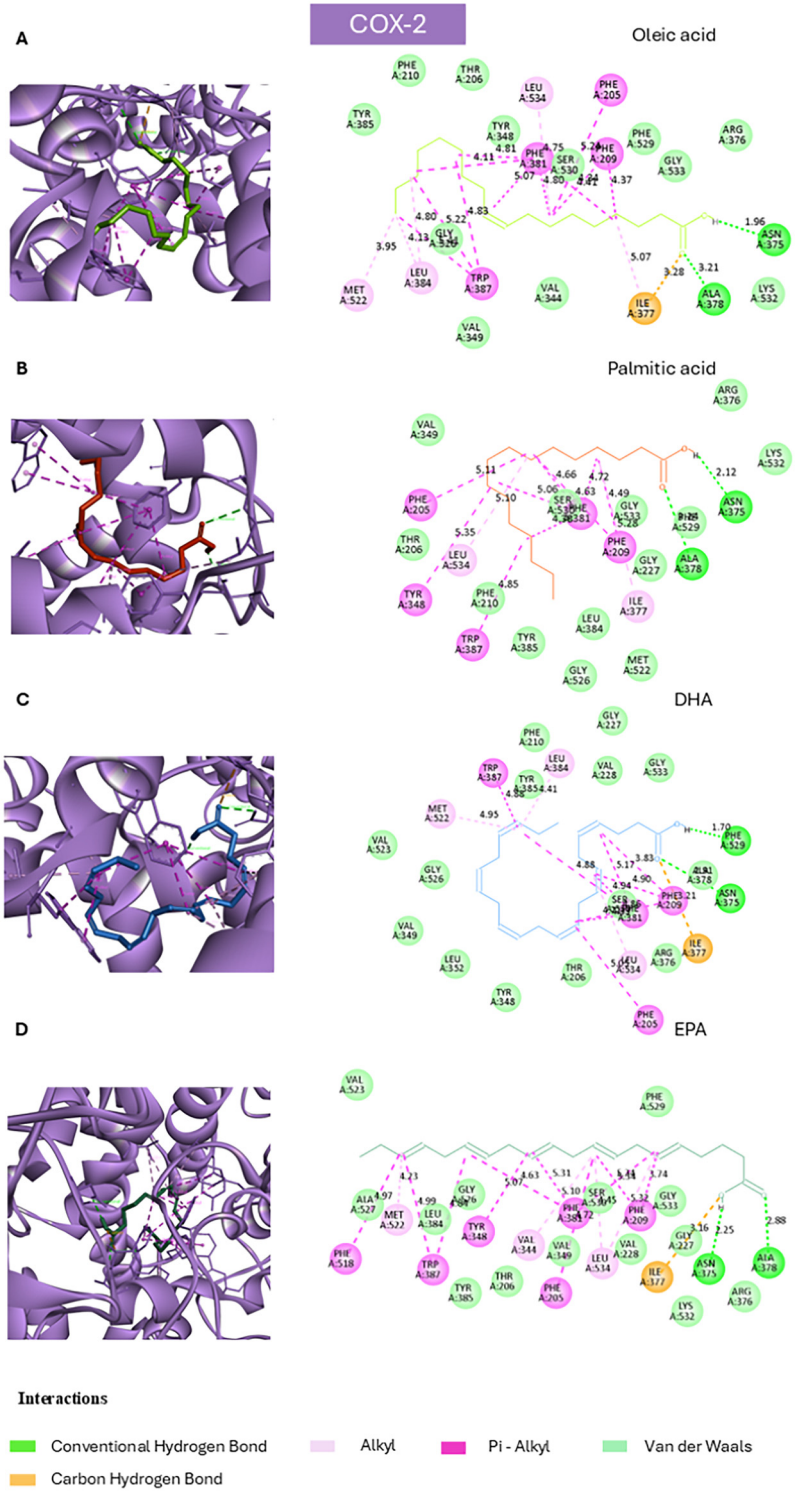

Fig. 8 Binding poses and interaction fingerprints of dietary fatty acids in the cyclooxygenase-2 (COX-2; PDB 1DDX) arachidonic-acid channel. Left panels: best-scoring docked poses within the arachidonate-binding channel of COX-2. Right panels: corresponding 2D interaction diagrams (hydrogen bonds, π/alkyl and alkyl contacts, and van der Waals) generated in BIOVIA Discovery Studio Visualizer. (A) Oleic acid–COX-2; (B) palmitic acid–COX-2; (C) DHA–COX-2; (D) EPA–COX-2. Poses occupy the elongated hydrophobic channel with engagement of lining residues consistent with arachidonate accommodation, in line with a non-covalent, channel-filling binding mode. All renderings used identical visualization parameters.

This journal is © The Royal Society of Chemistry 2026

Open Access Article. Published on 17 April 2026. Downloaded on 5/30/2026 11:00:16 AM.
This article is licensed under a Creative Commons Attribution-NonCommercial 3.0 Unported Licence.

transporters, antioxidative enzymes) or live-cell indicators of calcium dynamics would refine mechanistic inference. In addition, the observation window is short; extending dietary exposure and the post-challenge interval would help to test the durability of the EVOO advantage over refined MUFA, and to determine whether ω3-LCPUFA and EVOO exert additive or mechanistically distinct modes of astroglial control. Even within these bounds, Fig. 4 demonstrates that dietary fat quality and matrix strongly condition astrocyte responses to cholinergic stress, with ω3-LCPUFA showing the most favourable profile and EVOO a close second, whereas SFA confers the least protection.

3.4. Molecular docking suggests a biochemical rationale for PUFA superiority and EVOO advantages

The docking dataset outlines a coherent target-level framework that mirrors the *in vivo* hierarchy, DHA/EPA > oleic ≥ palmitic, and offers mechanistic nuances for why ω3-LCPUFA feeding and, secondarily, olive oil matrices confer advantages. In docking analyses of AChE, TREM2, BACE-1, and COX-2, DHA and EPA yielded the most favourable predicted binding free energies (Table 1), while oleic acid occupied functionally relevant surfaces with intermediate scores and palmitic acid generally trailed, consistent with a more limited interaction repertoire dominated by hydrophobic interactions. For AChE, which governs synaptic acetylcholine tone in the scopolamine paradigm,[38] DHA (−7.4 kcal mol^{-1}) and EPA (−7.6 kcal mol^{-1}) outperformed oleic (−5.9 kcal mol^{-1}) and palmitic (−6.5 kcal mol^{-1}) acids. Poses clustered in the peripheral anionic site (PAS) rather than establishing a credible catalytic geometry at the Ser203-His447-Glu334 triad; all ligands engaged canonical PAS residues (*e.g.*, Tyr72, Trp86, Tyr124, Trp286, Phe295, Tyr337, Phe338), whereas only the SFAs/MUFAs occasionally approached the triad without forming catalytically competent contacts (Fig. 5).[39] This PAS-biased pattern suggests non-catalytic modulation, a plausible route to mitigate scopolamine-induced dysfunction, rather than classical active site inhibition, thus providing a mechanistic bridge to the cholinergic layer of our *in vivo* readouts.

For TREM2, all fatty acids were localized to the apoE-interacting surface of the ectodomain, a lipid-sensing patch implicated in agonist responses;[21] EPA (−8.0 kcal mol^{-1}) scored highest, with oleic and palmitic (−7.7 kcal mol^{-1}) acids, and DHA (−7.4 kcal mol^{-1}) close behind (Fig. 6). Although top-ranked poses did not form a specific salt bridge to Arg47, their consistent occupancy of this agonist-responsive interface is compatible with allosteric stabilization of microglial TREM2 signalling. This aligns with the broadly reduced microglial markers observed across HFDs and suggests that quality-dependent differences may require longer exposure or disease-progressive models to surface histologically. For BACE1, the aspartyl protease that initiates the amyloidogenic pathway by cleaving APP at the β-site, ultimately leading to the formation of amyloid-β peptides,[40] EPA (−8.4 kcal mol^{-1}) and DHA (−8.5 kcal mol^{-1}) again surpassed oleic (−6.9 kcal mol^{-1}) and palmitic (−6.8 kcal mol^{-1}) acids (Fig. 7). Poses occupied the catalytic cleft but primarily made van der Waals contacts with the Asp32-Asp228 dyad, while establishing interactions with lining residues (*e.g.*, Thr72 hydrogen bonds; Phe108 π-alkyl/aromatic contacts).[41] This is compatible with substrate-gating or micro-allosteric effects rather than tight competitive inhibition, consistent with a scenario in which ω3-LCPUFA-rich environments subtly influence APP processing in concert with membrane remodelling. Finally, COX-2 displayed the strongest absolute scores, led by DHA (−10.5 kcal mol^{-1}) and EPA (−9.8 kcal mol^{-1}); notably, oleic acid (−9.2 kcal mol^{-1}) also docked favourably relative to palmitic acid (−8.3 kcal mol^{-1}) within the arachidonate-binding channel (Fig. 8). Ligands engaged a network of hydrophobic and aromatic contacts (including Trp387, among others)[42] and carboxylate-compatible interactions near the channel entrance. This rank order is consistent with the idea that highly unsaturated fatty acid chains interact more efficiently with the elongated channel, providing a mechanistic basis for the modulation of eicosanoid and inflammation-resolution pathways under ω3-LCPUFA feeding.[43] Collectively, this evidence on composition, binding and function strengthens the translational rationale for prioritising ω3-LCPUFA and high-quality olive oils as dietary strategies to modulate neuroinflammation and amyloid-relevant axis *in vivo*, while underscoring the need for biophysical and biochemical validation in membrane-mimetic systems to define these interaction maps.

4. Conclusions

Dietary fat quality, beyond total fat, emerged as a key determinant of brain immune tone in a scopolamine-induced, Alzheimer's-like context. ω3-LCPUFA feeding consistently dampened astroglial reactivity and restored a more physiological, ramified morphology, while EVOO-MUFA conferred advantages over refined MUFA, consistent with matrix/phenolic co-factors. By contrast, microglial markers (Iba-1, TNF-α, COX-2) were broadly attenuated across HFDs, suggesting a dominant effect of lipid availability on acute neuroinflammatory set-points in this short, high-amplitude window. Complementary structure-based docking offered a mechanistic framework: EPA/DHA showed the strongest predicted engagement at COX-2 and BACE1, whereas MUFA/SFA occupied functionally relevant regions on AChE (PAS) and TREM2 (apoE-responsive surface), outlining plausible eicosanoid, amyloid, cholinergic and microglial-sensing axes by which diet can shape neuroimmune signalling. Together, these lines of evidence support a composition, binding, and function framework in which PUFA-rich and EVOO-based diets buffer neuroinflammation pertinent to AD. This work has boundaries, notably an acute cholinergic paradigm, rigid-receptor docking without explicit membranes, and limited readouts of neuronal integrity, but the internal directionality is coherent and actionable. We propose targeted lipidomics and eicosanoid/pro-resolving mediator profiling to test

Open Access Article. Published on 17 April 2026. Downloaded on 5/30/2026 11:00:16 AM.
This article is licensed under a Creative Commons Attribution-NonCommercial 3.0 Unported Licence.

whether COX-2–linked networks mirror the predicted hierarchy; TREM2 signalling assays and BACE1 enzymology in progressive amyloid/tau models to examine causality; and factorial designs separating fatty-acid class from EVOO phenolics to quantify matrix co-drivers. A limitation is that EPA/DHA was administered in combination with a MUFA-rich oil (ROO), which increases nutritional realism but does not allow us to isolate the effect of fish oil as the sole fat source. Overall, the findings strengthen the translational rationale for precision nutrition strategies, prioritising ω3-LCPUFA and high-quality olive oils to modulate neuroinflammation and potentially slow trajectories relevant to AD.

Author contributions

Conceptualization, C. M. C.-C., S. M.-d. l. P.; methodology, L. B.-C., M. A., T. G.-d. l. R., M. D. N.-H.; formal analysis, T. G.-d. l. R., E. M.-P., M. T.-L.; investigation, J. L. d. l. R.-V., T. G.-d. l. R., S. M.-d. l. P.; resources, S. M.-d. l. P.; writing – original draft preparation, M. A.; writing – review and editing, S. M.-d. l. P.; supervision, S. M.-d. l. P.; funding acquisition, S. M.-d. l. P. All authors have read and agreed to the published version of the manuscript.

Conflicts of interest

The authors declare that they have no known competing financial interests or personal relationships that could have appeared to influence the work reported in this paper.

Data availability

The data supporting this article have been included as part of the supplementary information (SI). Supplementary information is available. See DOI: https://doi.org/10.1039/d6fo00279j.

Acknowledgements

This publication is part of the project PID2022-138650OA-I00, funded by MICIU/AEI/10.13039/501100011033 and by ERDF/EU. Luna Barrera-Chamorro has the benefit of a doctoral fellowship supported by the VII Program of Inner Initiative for Research and Transfer of University of Seville (VII-PPIT-US). Teresa Gonzalez-de la Rosa, Maria Torrecillas-Lopez, and Elvira Marquez-Paradas have the benefit of a doctoral fellowship from the Spanish Ministry of Science, Innovation, and Universities (FPU23/02652, PREP2022–000408, and FPU22/01097, respectively). Jose L. del-Rio-Vazquez is supported by a research contract funded by the project PID2022-138650OA-I00, granted by MCIN/AEI/10.13039/501100011033. Maria D. Navarro-Hortal is supported by a Juan de la Cierva Grant with reference number JDC2023-050414-I, funded by AEI/10.13039/501100011033 and the FSE+.

References

1 J. P. Ferrari-Souza, G. Povala, N. Rahmouni, B. Bellaver, P. C. L. Ferreira, M. A. De Bastiani, *et al.*, Microglia modulate Aβ-dependent astrocyte reactivity in Alzheimer's disease, *Nat. Neurosci.*, 2026, **29**, 81–87, DOI: 10.1038/s41593-025-02103-0.

2 F. Yin, Lipid metabolism and Alzheimer's disease: clinical evidence, mechanistic link and therapeutic promise, *FEBS J.*, 2023, **290**, 1420–1453, DOI: 10.1111/febs.16344.

3 E. Grao-Cruces, C. M. Claro-Cala, S. Montserrat-De la Paz and C. Nóbrega, Lipoprotein metabolism, protein aggregation, and Alzheimer's disease: a literature review, *Int. J. Mol. Sci.*, 2023, **24**, 2944, DOI: 10.3390/ijms24032944.

4 F. Rivero-Pino, E. Grao-Cruces, S. Lopez-Enriquez, G. Alba, E. Marquez-Paradas, C. M. Claro-Cala, C. Santa-Maria and S. Montserrat-De la Paz, Modulation of beta-amyloid-activated primary human neutrophils by dietary phenols from virgin olive oil, *Nutrients*, 2023, **15**, 941, DOI: 10.3390/nu15040941.

5 R. Toscano, M. C. Millan-Linares, A. Lemus-Conejo, C. Claro, V. Sanchez-Margalet and S. Montserrat-De la Paz, Postprandial triglyceride-rich lipoproteins promote M1/M2 microglia polarization in a fatty-acid-dependent manner, *J. Nutr. Biochem.*, 2020, **75**, 108248, DOI: 10.1016/j.jnutbio.2019.108248.

6 A.-J. Tessier, M. Cortese, C. Yuan, K. Bjornevik, A. Ascherio, D. D. Wang, J. E. Chavarro, M. J. Stampfer, F. B. Hu, W. C. Willett and M. Guasch-Ferré, Consumption of olive oil and diet quality and risk of dementia-related death, *JAMA Netw. Open*, 2024, **7**, e2410021, DOI: 10.1001/jamanetworkopen.2024.10021.

7 M. Poxleitner, S. H. L. Hoffmann, G. Berezhnoy, T. M. Ionescu, I. Gonzalez-Menendez, F. C. Maier, *et al.*, Western diet increases brain metabolism and adaptive immune responses in a mouse model of amyloidosis, *J. Neuroinflammation*, 2024, **21**, 129, DOI: 10.1186/s12974-024-03080-0.

8 L. Barrera-Chamorro, A. Fernandez-Prior, C. M. Claro-Cala, J. L. del Rio-Vazquez, F. Rivero-Pino and S. Montserrat-De la Paz, Unveiling the neuroprotective impact of virgin olive oil ingestion via the microbiota–gut–brain axis, *Food Funct.*, 2025, **16**, 24–39, DOI: 10.1039/D4FO04560B.

9 M. E. Traetta, H. A. Vecchiarelli and M.-È. Tremblay, Fundamental neurochemistry review: lipids across microglial states, *J. Neurochem.*, 2025, **169**, e16259, DOI: 10.1111/jnc.16259.

10 M. Slayo, C. Rummel, P. H. Singhaarachchi, M. Feldotto and S. J. Spencer, The role of n-3-derived specialised pro-resolving mediators (SPMs) in microglial mitochondrial respiration and inflammation resolution in Alzheimer's disease, *Mol. Neurodegener.*, 2025, **20**, 35, DOI: 10.1186/s13024-025-00824-1.

11 Y. Chen, R. Touboul, Y. Chen and C. L. Chang, Strategic delivery of omega-3 fatty acids for modulating inflamma-

Open Access Article. Published on 17 April 2026. Downloaded on 5/30/2026 11:00:16 AM. This article is licensed under a Creative Commons Attribution-NonCommercial 3.0 Unported Licence.

tory neurodegenerative diseases, *Front. Aging Neurosci.*, 2025, **17**, 1535094, DOI: 10.3389/fnagi.2025.1535094.

12 A. Cañuelo, Olive polyphenols as modulators of amyloid aggregation: mechanisms and implications for neurodegenerative diseases, *Food Funct.*, 2025, **16**, 8658–8679, DOI: 10.1039/D5FO03331D.

13 F. Rivero-Pino, Oleocanthal – characterization, production, safety, functionality and in vivo evidences, *Food Chem.*, 2023, **425**, 136504, DOI: 10.1016/j.foodchem.2023.136504.

14 R. Zupo, F. Castellana, F. Panza, V. Solfrizzi, M. Lozupone, R. Tardugno, *et al.*, Alzheimer's disease may benefit from olive oil polyphenols: a systematic review on preclinical evidence supporting the effect of oleocanthal on amyloid-β load, *Curr. Neuropharmacol.*, 2025, **23**, 1249–1259, DOI: 10.2174/011570159X327650241021115228.

15 G. C. De Paula, B. I. Aldana, R. Battistella, R. Fernández-Calle, A. Bjure, I. Lundgaard, T. Deierborg and J. M. N. Duarte, Extracellular vesicles released from microglia after palmitate exposure impact brain function, *J. Neuroinflammation*, 2024, **21**, 173, DOI: 10.1186/s12974-024-03168-7.

16 P. Prakash, C. E. Randolph, K. A. Walker and G. Chopra, Lipids: emerging players of microglial biology, *Glia*, 2025, **73**, 657–677, DOI: 10.1002/glia.24654.

17 S. De Chiara, L. De Simone Carone, R. Cirella, E. Andretta, A. Silipo, A. Molinaro, M. Mercogliano and F. Di Lorenzo, Beyond the Toll-like receptor 4: structure-dependent lipopolysaccharide recognition systems—how far are we?, *ChemMedChem*, 2025, **20**, e202400780, DOI: 10.1002/cmdc.202400780.

18 S. Vittorio, F. Lunghini, P. Morerio, D. Gadioli, S. Orlandini, P. Silva, *et al.*, Addressing docking pose selection with structure-based deep learning: recent advances, challenges and opportunities, *Comput. Struct. Biotechnol. J.*, 2024, **23**, 2141–2151, DOI: 10.1016/j.csbj.2024.05.024.

19 F. Rivero-Pino, T. Gonzalez-De la Rosa, M. Torrecillas-Lopez, L. Barrera-Chamorro, J. L. Del Rio Vazquez, E. Marquez-Paradas, *et al.*, Characterization of Rugulopteryx okamurae algae: a source of bioactive peptides, omega-3 fatty acids, and volatile compounds, *Food Chem.*, 2025, **473**, 143084, DOI: 10.1016/j.foodchem.2025.143084.

20 M. Torrecillas-Lopez, C. M. Claro-Cala, T. Gonzalez-De la Rosa, L. Barrera-Chamorro, M. C. Millan-Linares, E. Marquez-Paradas, A. Villanueva, J. L. Del Rio-Vazquez and S. Montserrat-De la Paz, Neuroavailable peptides from hempseed protein hydrolysates reduce hippocampal inflammation and glial activation in a scopolamine-induced Alzheimer's disease model, *Biomed. Pharmacother.*, 2025, **191**, 118438, DOI: 10.1016/j.biopha.2025.118438.

21 Z. Mai, W. Wei, H. Yu, Y. Chen, Y. Wang and Y. Ding, Molecular recognition of the interaction between ApoE and the TREM2 protein, *Transl. Neurosci.*, 2022, **13**, 93–103, DOI: 10.1515/tnsci-2022-0218.

22 J. Wen, S. K. Satyanarayanan, A. Li, L. Yan, Z. Zhao, Q. Yuan, *et al.*, Unraveling the impact of omega-3 polyunsaturated fatty acids on blood–brain barrier integrity and glymphatic function, *Brain, Behav., Immun.*, 2024, **115**, 335–355, DOI: 10.1016/j.bbi.2023.10.018.

23 S. Lopez, B. Bermudez, S. Montserrat-De la Paz, S. Jaramillo, L. M. Varela, A. Ortega-Gomez, R. Abia and F. J. G. Muriana, Membrane composition and dynamics: a target of bioactive virgin olive oil constituents, *Biochim. Biophys. Acta, Biomembr.*, 2014, 1638–1656, DOI: 10.1016/j.bbamem.2014.01.007.

24 M. Slayo, C. Rummel, P. H. Singhaarachchi, M. Feldotto, S. J. Spencer, G. M. Pasinetti, *et al.*, The role of n-3-derived specialised pro-resolving mediators (SPMs) in microglial mitochondrial respiration and inflammation resolution in Alzheimer's disease, *Mol. Neurodegener.*, 2025, **20**, 35, DOI: 10.1186/s13024-025-00824-1.

25 M. Poxleitner, S. H. L. Hoffmann, G. Berezhnoy, T. M. Ionescu, I. González-Méndez, F. C. Maier, *et al.*, Western diet increases brain metabolism and adaptive immune responses in a mouse model of amyloidosis, *J. Neuroinflammation*, 2024, **21**, 129, DOI: 10.1186/s12974-024-03080-0.

26 A. Jagielska, K. Sałaciak and K. Pytka, Beyond the blur: scopolamine's utility and limits in modeling cognitive disorders across sexes—narrative review, *Ageing Res. Rev.*, 2025, **104**, 102635, DOI: 10.1016/j.arr.2024.102635.

27 A. S. Warden, C. Han, E. Hansen, S. Trescott, C. Nguyen, R. Kim, *et al.*, Tools for studying human microglia: in vitro and in vivo strategies, *Brain, Behav., Immun.*, 2023, **107**, 369–382, DOI: 10.1016/j.bbi.2022.10.008.

28 F. Ren, Y. Luo, P. Liu, H. Xiong, X. Liu and J. Wang, The role of TNF signaling pathway in post-stroke cognitive impairment: a systematic review, *Ann. Med.*, 2025, **57**, 2543519, DOI: 10.1080/07853890.2025.2543519.

29 H. Ni, Z. Guo, Y. Wu, J. Wang, Y. Yang, Z. Zhu and D. Wang, The crucial role that hippocampus cyclooxygenase-2 plays in memory, *Eur. J. Neurosci.*, 2023, **58**, 4123–4136, DOI: 10.1111/ejn.16165.

30 C.-H. Hsu, Y.-Y. Hsu, B.-M. Chang, K. Raffensperger, M. Kadden, H. T. Ton, *et al.*, StainAI: quantitative mapping of stained microglia and insights into brain-wide neuroinflammation and therapeutic effects in cardiac arrest, *Commun. Biol.*, 2025, **8**, 462, DOI: 10.1038/s42003-025-07926-y.

31 T. Hu, C.-H. Liu, M. Lei, Q. Zeng, L. Li, H. Tang, *et al.*, Metabolic regulation of the immune system in health and diseases: mechanisms and interventions, *Signal Transduction Targeted Ther.*, 2024, **9**, 268, DOI: 10.1038/s41392-024-01954-6.

32 M. Cerasuolo, I. Di Meo, M. C. Auriemma, G. Paolisso, M. Papa and M. R. Rizzo, Exploring the dynamic changes of brain lipids, lipid rafts, and lipid droplets in aging and Alzheimer's disease, *Biomolecules*, 2024, **14**, 1362, DOI: 10.3390/biom14111362.

Open Access Article. Published on 17 April 2026. Downloaded on 5/30/2026 11:00:16 AM.
This article is licensed under a Creative Commons Attribution-NonCommercial 3.0 Unported Licence.

33 T. Hu, C.-H. Liu, M. Lei, Q. Zeng, L. Li, H. Tang, *et al.*, Metabolic regulation of the immune system in health and diseases: mechanisms and interventions, *Signal Transduction Targeted Ther.*, 2024, **9**, 268, DOI: 10.1038/s41392-024-01954-6.

34 M. L. Longarzo, A. d'Ambrosio, R. Di Salle, C. Tedeschi, G. Esposito, F. Sorrentino, *et al.*, Understanding the effects of omega-3 fatty acid supplementation on brain membrane organization, *Prog. Neuro-Psychopharmacol. Biol. Psychiatry*, 2024, **127**, 110530, DOI: 10.1016/j.pnpbp.2024.110530.

35 H. Wang, Y. Liu, K. Zhao, P. Li, J. Xu, W. Li, *et al.*, Connexin43 and its regulation of astrocyte gap junction coupling: implications for CNS disease, *Front. Cell Dev. Biol.*, 2025, **13**, 1543981, DOI: 10.3389/fcell.2025.1543981.

36 J.-P. Schuchardt, C. M. Hahn, U. Hahn and A. Hahn, Omega-3 supplementation changes the physical properties of immune-cell membranes, *Prostaglandins, Leukotrienes Essent. Fatty Acids*, 2024, **198**, 102686, DOI: 10.1016/j.plefa.2024.102686.

37 L. Wei, H. Zhang, C. Li, Y. Sun, F. Chen, Q. Liu, *et al.*, Neuroprotective properties of extra-virgin olive oil polyphenols: mechanisms and translational outlook, *Nutrients*, 2025, **17**, 3987, DOI: 10.3390/nu17113987.

38 N. Himaja, J. Niveditha, L. Hu, P. K. Deb, Q. Liu, X. Xue, *et al.*, Development of the "hidden" multi-target-directed ligands by AChE/BuChE for the treatment of Alzheimer's disease, *Eur. J. Med. Chem.*, 2023, **251**, 115253, DOI: 10.1016/j.ejmech.2023.115253.

39 Y. Wan, S. Guan, M. Qian, H. Huang, F. Han, S. Wang, *et al.*, Structural basis of fullerene derivatives as novel potent inhibitors of protein acetylcholinesterase without catalytic active site interaction: insight into the inhibitory mechanism through molecular modeling studies, *J. Biomol. Struct. Dyn.*, 2020, **38**, 410–425, DOI: 10.1080/07391102.2019.1576543.

40 K. L. C. Monteiro, M. G. S. Alcântara, N. M. L. Freire, E. M. Brandão, V. L. do Nascimento, L. M. D. S. Viana, *et al.*, BACE-1 Inhibitors Targeting Alzheimer's Disease, *Curr. Alzheimer Res.*, 2023, **20**, 131–148, DOI: 10.2174/1567205020666230612155953.

41 A. K. Ghosh and J. Tang, Discovery of Cyclic Sulfone Hydroxyethylamines as Potent and Selective β-Site APP-Cleaving Enzyme 1 (BACE1) Inhibitors: Structure-Based Design and in Vivo Reduction of Amyloid β-Peptides, *J. Med. Chem.*, 2012, **55**, 9425–9441, DOI: 10.1021/jm300069y.

42 J. R. Kiefer, J. L. Pawlitz, K. T. Moreland, R. A. Stegeman, W. F. Hood, J. K. Gierse, *et al.*, Structural insights into the stereochemistry of the cyclooxygenase reaction, *Nature*, 2000, **405**, 97–101, DOI: 10.1038/35011103.

43 M. Shah, R. Parmar, K. Patel and A. Nagani, Indole-based COX-2 inhibitors: A decade of advances in inflammation, cancer, and Alzheimer's therapy, *Bioorg. Chem.*, 2024, **153**, 107931, DOI: 10.1016/j.bioorg.2024.107931.

This journal is © The Royal Society of Chemistry 2026